Electroactive Biofilms

DOI: 10.1002/ange.201400463

Highly Active Bidirectional Electron Transfer by a Self-Assembled Electroactive Reduced-Graphene-Oxide-Hybridized Biofilm**

*Yang-Chun Yong, Yang-Yang Yu, Xinhai Zhang, and Hao Song**

Abstract: *Low extracellular electron transfer performance is often a bottleneck in developing high-performance bioelectrochemical systems. Herein, we show that the self-assembly of graphene oxide and Shewanella oneidensis MR-1 formed an electroactive, reduced-graphene-oxide-hybridized, three-dimensional macroporous biofilm, which enabled highly efficient bidirectional electron transfers between Shewanella and electrodes owing to high biomass incorporation and enhanced direct contact-based extracellular electron transfer. This 3D electroactive biofilm delivered a 25-fold increase in the outward current (oxidation current, electron flux from bacteria to electrodes) and 74-fold increase in the inward current (reduction current, electron flux from electrodes to bacteria) over that of the naturally occurring biofilms.*

Microbial electrochemical systems (MES), including microbial fuel cells (MFC),[1] microbial electrolysis cells (MEC),[2] microbial reverse-electrodialysis cells,[3] and microbial electrosynthesis (MESy),[4] are appealing for capturing energy from organic waste and converting waste into commodity chemicals.[5] Bacterial extracellular electron transfer (EET), which dictates the exchange of electrons between exoelectrogenic bacteria and electrodes is a bottleneck in determining the efficiency of MES. Low EET efficiency continues to limit the practical application of MES.

Electrochemically active biofilms, highly structured microbial communities attached to electrodes, play crucial roles in the EET of bacteria.[5–6] Biofilms can substantially facilitate EET between bacteria and electrodes superior to that of planktonic bacteria, owing to their higher local cell density, potentially higher local electron shuttles concentration, shorter EET distance, and the involvement of direct electron transfer pathways through c-type cytochromes.[6c,7] In view of this, various electrode materials have been developed to increase biofilm formation, including biocompatible surface decoration and three-dimensional macroporous electrodes with enhanced surface areas.[8] In particular, graphene-based materials were recently adopted in MFC anodes to improve their performance by taking advantage of the unique properties of graphene, including outstanding electrical conductivity, extremely high specific surface area, mechanical robustness and flexibility, chemical inertness, and biocompatibility.[8a,b,9] However, low total biomass loading of naturally formed biofilms on these electrode surfaces limits further improvement of energy output in MFCs and performance of other MES.[6c,10]

Herein, a self-assembled 3D reduced graphene oxide (rGO)/bacteria hybrid biofilm was constructed by the one-step self-assembly of *Shewanella oneidensis* MR-1 and water-soluble graphene oxide (GO) coupled with in situ bioreduction of non-conductive GO to conductive rGO by the bacteria (Scheme 1). The bacterial cells were captured by the GO nanosheets by a "fishing" process,[11] where the GO nanosheets acted as nets to catch the bacterial "fish" (Scheme 1 a). The GO nanosheets were then reduced to rGO, and self-assembled to form a 3D macroporous network. This enabled the incorporation of a large amount bacteria into the biofilm matrix, and formed multiplexed conductive pathways, thus facilitating EET between bacteria and electrode (Scheme 1 b). Thus, this 3D hybrid biofilm exhibited an extraordinarily high electrochemical activity, and outperformed naturally occurring biofilms in bidirectional EET.

The 3D biofilm was self-assembled by mixing *S. oneidensis* MR-1 with a GO solution in the anodic chamber of a dual-chamber MFC. Slow stirring (50 rpm) to give gentle mixing of the bacteria suspension and GO enabled a gradual attachment of the GO/bacteria hybrid onto the carbon cloth electrode. After two days of incubation, the anolyte turned black and aggregates formed, suggesting GO (brown, water soluble) was reduced to rGO (black, water insoluble).[12] After nine days of incubation, a thick (ca. 4.5 mm) rGO/

[*] Prof. Y. C. Yong
Biofuels Institute, School of the Environment, Jiangsu University, 301 Xuefu Road, Zhenjiang 212013, Jiangsu Province (China)
Y. Y. Yu, Prof. H. Song
School of Chemical and Biomedical Engineering, and Singapore Centre on Environmental Life Sciences Engineering, Nanyang Technological University, Singapore 637457 (Singapore)
E-mail: songhao@ntu.edu.sg
Prof. X. Zhang
Department of Electrical and Electronic Engineering, South University of Science and Technology of China, 1088 Xueyuan Road Xili, Nanshan District, Shenzhen, Guangdong 518055 (China)
Prof. H. Song
Key Laboratory of Systems Bioengineering, Ministry of Education, School of Chemical Engineering & Technology, and Collaborative Innovation Center of Chemical Science and Engineering (Tianjin), Tianjin University, Tianjin 300072 (China)
E-mail: hsong@tju.edu.cn

[**] This research was supported by the Ministry of Science and Technology of China (973 Program: 2014CB745100), the National Natural Science Foundation of China (21306069, 21376174), the Ministry of Science and Technology of China (863 Program: 2012AA02A701), the Natural Science Foundation of Jiangsu Province (13K20130492), the "Six Talent Peaks" program (2012-NY-029, Jiangsu Province, China), an AcRF Tier-1 grant (RG 78/10, MOE, Singapore), an AcRF Tier-2 grant (MOE2011-T2-2-035), and The Environment and Water Industry Programme Office of Singapore.

Supporting information for this article is available on the WWW under http://dx.doi.org/10.1002/anie.201400463.

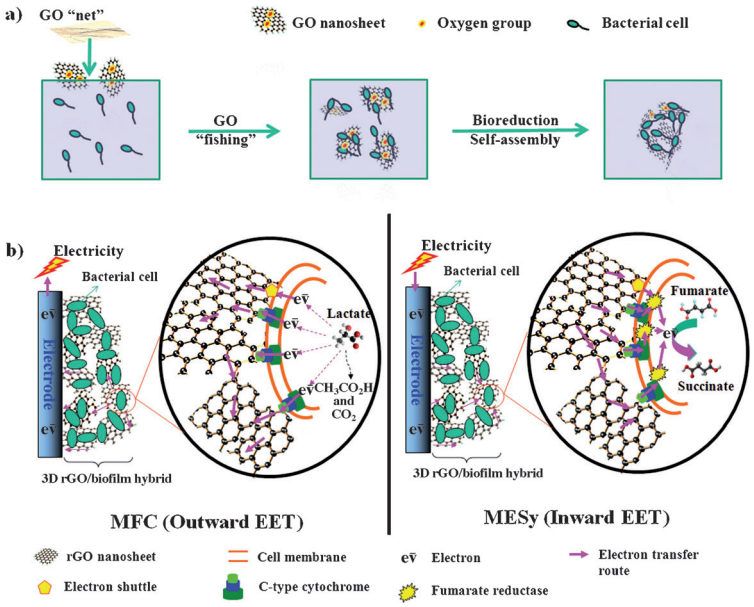

Scheme 1. Self-assembly of the 3D macroporous rGO/bacteria hybrid biofilm by a fishing process (a), and the proposed mechanism of bidirectional EET (b).

Shewanella hybrid biofilm was firmly attached to the electrode. In the absence of GO, only a thin (roughly single) layer of *Shewanella* biofilm (i.e., a naturally occurring control biofilm) formed on the carbon cloth anode (Supporting Information, Figure S1). Field-emission scanning electron microscopy (FESEM) images of the rGO/*Shewanella* hybrid biofilm showed a 3D macroporous interconnected rGO network (with pore sizes of 10–200 μm) (Figure 1 a,b), which guaranteed network conductivity and unhindered substrate transport. A firm attachment of bacteria to the surface of the graphene nanosheets was observed (Figures 1 c and S1).

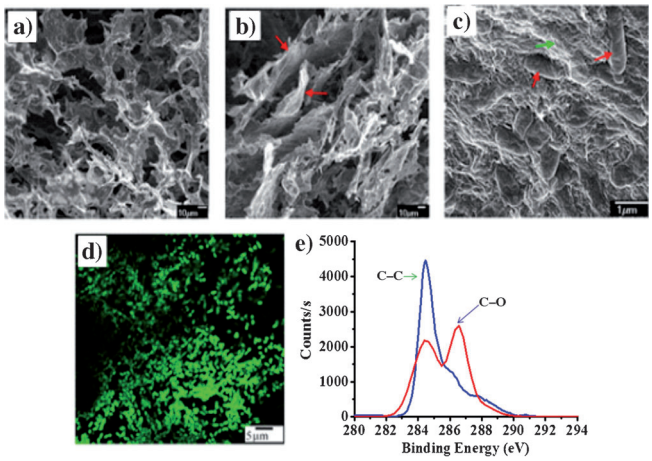

Figure 1. a–c) FESEM images of the 3D rGO/*Shewanella* hybrid biofilm. a) View from the upper surfaces of the 3D biofilm (scale bar = 10 μm). b) Side view of the 3D biofilm, red arrows indicate rGO nanosheets (scale bar = 10 μm). c) Cells (red arrows) tightly anchored onto rGO surfaces (green arrow; scale bar = 1 μm)). d) CSLM image of the 3D biofilm (scale bar = 5 μm). e) The C1s XPS spectra of the GO starting material and rGO from the 3D biofilm. rGO (blue), GO (red).

There have been contradictory reports on the biocompatibility of GO and rGO.[13] Here, the rGO-hybrid 3D biofilm can continuously generate electric current in MFCs for at least one month, suggesting high viability of cells in the biofilm. The bacterial viability was further examined after MFC discharge by confocal scanning laser microscopy (CSLM) stained with the LIVE/DEAD BacLight bacterial viability kit. Viable cells (green fluorescence) covered nearly the entire area of the graphene nanosheets, with negligible red fluorescence by dead cells (Figure 1 d). Thus, the tight adhesion of the highly viable *Shewanella* cells to the surfaces of the rGO nanosheets (Figures 1 c and S1), together with its 3D macroporous structure (Figure 1 a,b) ensured high biomass loading and facilitated interaction between the bacteria and the rGO networks in the rGO/bacteria hybrid biofilm.

X-ray photoelectron spectroscopy (XPS), Raman spectroscopy, and Fourier transform infrared spectroscopy (FTIR) were further used to confirm the bioreduction of GO to rGO in the 3D biofilm. The C1s XPS spectrum of GO showed strong oxygenated peaks (e.g., C–O; Figure 1 e), thus indicating a considerable degree of oxidation in GO.[12a,14] In contrast, The C1s spectrum of the samples taken from the 3D rGO/*Shewanella* hybrid biofilm was dominated by a much stronger C–C peak, whereas the oxygenated C peaks (i.e., C–O) decreased tremendously (Figure 1 e); this is indicative of the formation of rGO.[12a,15] Raman and FTIR spectra also confirmed the reduction of GO in the 3D biofilm (Figures S2 and S3).

S. oneidensis MR-1 has two distinct pathways for EET: direct electron transfer through outer membrane c-type cytochromes and indirect transfer mediated by electron shuttles.[16] The tight anchoring of bacteria onto rGO nanosheets in the 3D biofilm dramatically decreased the EET distance of electron shuttles. Meanwhile, the large active surface area of the 3D rGO interlocked networks, and their intimate contact with cell membranes might enormously facilitate direct-contact-based EET. Cyclic voltammetry (CV) analysis showed that the 3D biofilm had a redox pair centered at about −0.32 V (Figure 2 a), which was more clearly observed in the baseline-subtracted CV plot (Figure 2 b). Differential pulse voltammetry (DPV) analysis further confirmed the existence of this redox pair (Figure S4), which is associated with the outer membrane c-type cytochromes of *S. oneidensis* MR-1.[9b] However, no detectable CV peaks were observed in the control biofilm (Figure 2 a). These outer membrane c-type cytochromes were involved in the electrocatalytic process of the 3D biofilm (Figure S5), which were barely detected in the CVs of many MFCs owing to their hindered electrochemical activity caused by their weak interactions with electrode materials.[8a,17,18] Thus, these electrochemical results suggested that the contact-based direct EET between *Shewanella* and the electrodes was enhanced, which the naturally occurring biofilms are incapable of. Moreover, electrochemical impedance spectroscopy (EIS) showed the charge-transfer resistance of the 3D biofilm

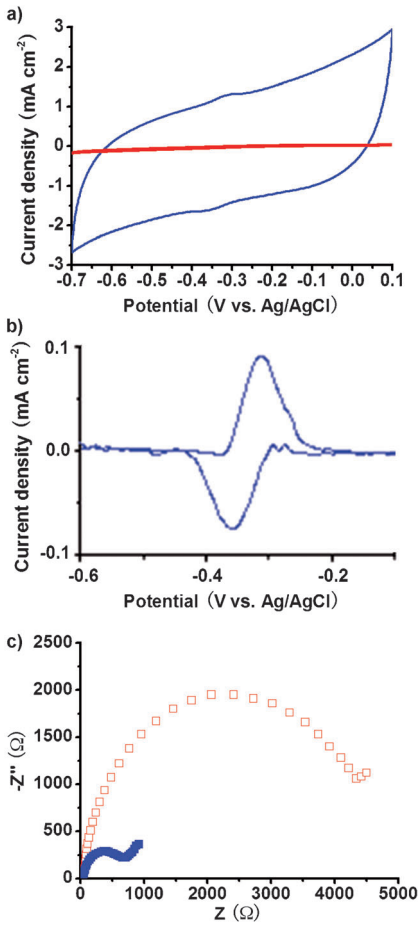

Figure 2. Cyclic voltammetry (a, b) at 30 mV s^{-1} and Nyquist plots (c) of the electrochemical impedance spectroscopy (scanned at 0.01–100 kHz at open-circuit potential, with a perturbation signal of 10 mV) of the 3D rGO/*Shewanella* hybrid biofilm (blue) and the control biofilm (red). (b) The baseline-subtracted CV plot for the 3D rGO/*Shewanella* hybrid biofilm.

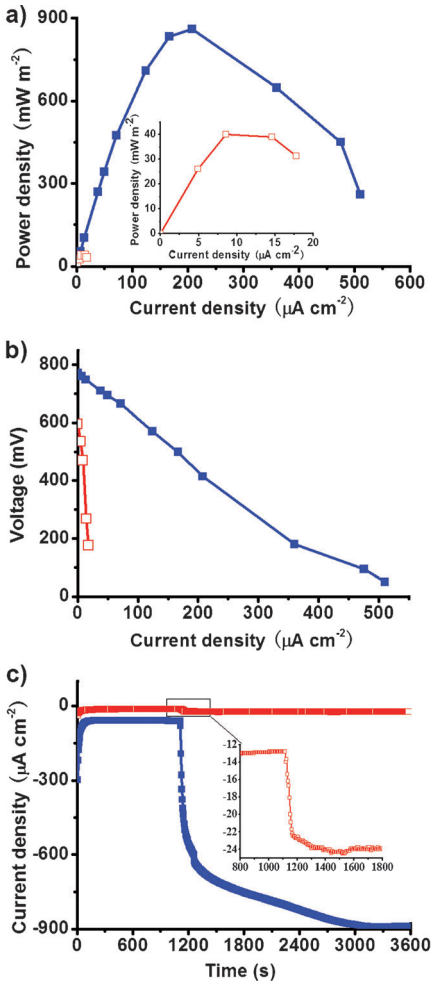

Figure 3. Power output curves (a; the inset depicts the enlarged view of the power output of the control biofilm) and polarization curves (b) of MFCs (outward EET). c) Current assimilation by *Shewanella* (inward EET) in the three-electrode microbial electrosynthesis system (MESy), in which the electrode potential was poised at −0.56 V (vs. Ag/AgCl), and fumarate (50 mM) was added at 1200 s (the inset is an expansion of the indicated region). 3D rGO/*Shewanella* hybrid biofilm (blue), control biofilm (red).

was ca. 750 Ω (the diameter of the semicircle in the Nyquist plot[19]), which is five times lower than that of the control biofilm (ca. 4500 Ω; Figure 2c); this indicates the much higher performance of EET in the 3D biofilm.

MFCs are associated with the bacterial outward transfer of intracellular electrons to extracellular electrodes (substrate oxidation).[1,5] The output voltage of the 3D biofilm reached an output voltage of 445 ± 20 mV ($n = 5$), which is ca. 3.5 times higher than that of the control biofilm (99 mV; Figure S6). The maximum power density achieved by the 3D biofilm was 843 ± 31 mW m^{-2} ($n = 3$), which is 22 times higher than that of the control biofilm (36 ± 7 mW m^{-2}, $n = 3$; Figure 3a).The maximum current output of the 3D biofilm measured by the polarization curve was 0.52 ± 0.12 mA cm^{-2} ($n = 3$), which is 25 times higher than that of the control biofilm (0.02 ± 0.01 mA cm^{-2}; Figure 3b). With the decrease of the externally loaded resistance, the output voltage of the 3D biofilm decreased much slower than that of the control (Figure 3b), thus indicating a smaller internal resistance was achieved because of the enhanced charge transfer rate.[8b] As summarized in Table S1, the performance of this MFC is clearly superior to previously reported MFCs using the same bacterial strain, similar MFC setups, but different anodes/biofilm matrices. In particular, this 3D biofilm MFC produced a ca. 100 mW m^{-2} higher power output than a sophisticated 3D graphene/polyaniline anode,[8a] and three times higher than conductive artificial biofilms.[20]

The microbial electrosynthesis process is driven by the inward electron transfer from electrodes to bacteria (substrate reduction).[2a,5] The inward electron flux is determined by the electricity consumption rate in the reduction of fumarate to succinate by *Shewanella* in a three-electrode electrochemical cell.[21] Upon addition of fumarate, both the control and the 3D biofilm showed a sudden onset of cathodic currents, suggesting electrons were assimilated and consumed by *Shewanella*.[21] The 3D biofilm reached a net current density change of 820 μA cm^{-2} (−60 to −880 μA cm^{-2}), which is ca. 74 times higher than that obtained by the control biofilm (−13 to −24 μA cm^{-2}; Figure 3c). The inward current den-

sities of these biofilms could maintain their steady-state level for at least a day (Figure S7).

In summary, a self-assembled 3D macroporous rGO/bacteria hybrid biofilm was constructed. Its increased loading of biomass, increased specific surface area, and electrochemical activity enabled an extraordinarily enhanced bidirectional electron transfer over that of naturally occurring biofilms, thus exhibiting promising applications in MFCs and microbial electrosynthesis.

Received: January 16, 2014
Published online: March 18, 2014

Keywords: biofilms · graphene · microbial electrosynthesis · microbial fuel cells · self-assembly

[1] D. R. Lovley, *Nat. Rev. Microbiol.* **2006**, *4*, 497 – 508.
[2] a) K. Rabaey, R. A. Rozendal, *Nat. Rev. Microbiol.* **2010**, *8*, 706 – 716; b) S. Cheng, B. E. Logan, *Proc. Natl. Acad. Sci. USA* **2007**, *104*, 18871 – 18873.
[3] R. D. Cusick, Y. Kim, B. E. Logan, *Science* **2012**, *335*, 1474 – 1477.
[4] H. Li, P. H. Opgenorth, D. G. Wernick, S. Rogers, T. Y. Wu, W. Higashide, P. Malati, Y. X. Huo, K. M. Cho, J. C. Liao, *Science* **2012**, *335*, 1596 – 1596.
[5] B. E. Logan, K. Rabaey, *Science* **2012**, *337*, 686 – 690.
[6] a) U. Schröder, *Phys. Chem. Chem. Phys.* **2007**, *9*, 2619 – 2629; b) G. Reguera, K. P. Nevin, J. S. Nicoll, S. F. Covalla, T. L. Woodard, D. R. Lovley, *Appl. Environ. Microbiol.* **2006**, *72*, 7345 – 7348; c) Y. C. Yong, Y. Y. Yu, C. M. Li, J. J. Zhong, H. Song, *Biosens. Bioelectron.* **2011**, *30*, 87 – 92.
[7] a) H. R. Luckarift, S. R. Sizemore, J. Roy, C. Lau, G. Gupta, P. Atanassov, G. R. Johnson, *Chem. Commun.* **2010**, *46*, 6048 – 6050; b) R. Nakamura, F. Kai, A. Okamoto, G. J. Newton, K. Hashimoto, *Angew. Chem.* **2009**, *121*, 516 – 519; *Angew. Chem. Int. Ed.* **2009**, *48*, 508 – 511.
[8] a) Y. C. Yong, X. C. Dong, M. B. Chan-Park, H. Song, P. Chen, *ACS Nano* **2012**, *6*, 2394 – 2400; b) Z. He, J. Liu, Y. Qiao, C. M. Li, T. T. Tan, *Nano Lett.* **2012**, *12*, 4738 – 4741; c) Y. J. Feng, Q. Yang, X. Wang, B. E. Logan, *J. Power Sources* **2010**, *195*, 1841 – 1844; d) V. Flexer, J. Chen, B. C. Donose, P. Sherrell, G. G. Wallace, J. Keller, *Energy Environ. Sci.* **2013**, *6*, 1291 – 1298; e) Y. Yuan, S. G. Zhou, Y. Liu, J. H. Tang, *Environ. Sci. Technol.* **2013**, *47*, 14525 – 14532; f) Y. Yuan, S. G. Zhou, B. Zhao, L. Zhuang, Y. Q. Wang, *Bioresour. Technol.* **2012**, *116*, 453 – 458.
[9] a) Y. Z. Zhang, G. Q. Mo, X. W. Li, W. D. Zhang, J. Q. Zhang, J. S. Ye, X. D. Huang, C. Z. Yu, *J. Power Sources* **2011**, *196*, 5402 – 5407; b) Y. X. Huang, X. W. Liu, J. F. Xie, G. P. Sheng, G. Y. Wang, Y. Y. Zhang, A. W. Xu, H. Q. Yu, *Chem. Commun.* **2011**, *47*, 5795 – 5797; c) X. Xie, G. H. Yu, N. Liu, Z. N. Bao, C. S. Criddle, Y. Cui, *Energy Environ. Sci.* **2012**, *5*, 6862 – 6866.
[10] a) H. S. Lee, C. I. Torres, B. E. Rittmann, *Environ. Sci. Technol.* **2009**, *43*, 7571 – 7577; b) H. C. Flemming, J. Wingender, *Nat. Rev. Microbiol.* **2010**, *8*, 623 – 633.
[11] W. F. Chen, S. R. Li, C. H. Chen, L. F. Yan, *Adv. Mater.* **2011**, *23*, 5679 – 5683.
[12] a) E. C. Salas, Z. Z. Sun, A. Luttge, J. M. Tour, *ACS Nano* **2010**, *4*, 4852 – 4856; b) H. L. Guo, X. F. Wang, Q. Y. Qian, F. B. Wang, X. H. Xia, *ACS Nano* **2009**, *3*, 2653 – 2659.
[13] a) O. N. Ruiz, K. A. Fernando, B. Wang, N. A. Brown, P. G. Luo, N. D. McNamara, M. Vangsness, Y. P. Sun, C. E. Bunker, *ACS Nano* **2011**, *5*, 8100 – 8107; b) W. B. Hu, C. Peng, W. J. Luo, M. Lv, X. M. Li, D. Li, Q. Huang, C. H. Fan, *ACS Nano* **2010**, *4*, 4317 – 4323.
[14] a) D. Yang, A. Velamakanni, G. Bozoklu, S. Park, M. Stoller, R. D. Piner, S. Stankovich, I. Jung, D. A. Field, C. A. Ventrice, R. S. Ruoff, *Carbon* **2009**, *47*, 145 – 152; b) G. M. Wang, F. Qian, C. Saltikov, Y. Q. Jiao, Y. Li, *Nano Res.* **2011**, *4*, 563 – 570.
[15] D. V. Kosynkin, A. L. Higginbotham, A. Sinitskii, J. R. Lomeda, A. Dimiev, B. K. Price, J. M. Tour, *Nature* **2009**, *458*, 872 – U875.
[16] a) X. C. Jiang, J. S. Hu, L. A. Fitzgerald, J. C. Biffinger, P. Xie, B. R. Ringeisen, C. M. Lieber, *Proc. Natl. Acad. Sci. USA* **2010**, *107*, 16806 – 16810; b) D. Coursolle, D. B. Baron, D. R. Bond, J. A. Gralnick, *J. Bacteriol.* **2010**, *192*, 467 – 474; c) Y. J. Xiong, L. Shi, B. W. Chen, M. U. Mayer, B. H. Lower, Y. Londer, S. Bose, M. F. Hochella, J. K. Fredrickson, T. C. Squier, *J. Am. Chem. Soc.* **2006**, *128*, 13978 – 13979.
[17] D. Baron, E. LaBelle, D. Coursolle, J. A. Gralnick, D. R. Bond, *J. Biol. Chem.* **2009**, *284*, 28865 – 28873.
[18] L. Peng, S. J. You, J. Y. Wang, *Biosens. Bioelectron.* **2010**, *25*, 1248 – 1251.
[19] Z. He, F. Mansfeld, *Energy Environ. Sci.* **2009**, *2*, 215 – 219.
[20] Y. Y. Yu, H. L. Chen, Y. C. Yong, D. H. Kim, H. Song, *Chem. Commun.* **2011**, *47*, 12825 – 12827.
[21] D. E. Ross, J. M. Flynn, D. B. Baron, J. A. Gralnick, D. R. Bond, *PLoS One* **2011**, *6*, e16649.

